JOURNAL OF APPLIED ELECTROCHEMISTRY **27** (1997) 784–792

Design of spectroelectrochemical cell for *in situ* X-ray absorption fine structure measurements of bulk solution species

M. R. ANTONIO*, L. SODERHOLM

Chemistry Division, Argonne National Laboratory, Argonne, IL, 60439–4831, USA

I. SONG

Department of Materials Science and Engineering, The Case School of Engineering, Case Western Reserve University, Cleveland, OH,44106–7204, USA

Received 5 February 1996

A purpose-built spectroelectrochemical cell for *in situ* fluorescence XAFS (X-ray absorption fine structure) measurements of bulk solution species is described. The cell performance was demonstrated by the collection of europium L_3-edge XANES (X-ray absorption near edge structure) during constant-potential electrolysis of 14.2 mM $EuCl_3.6H_2O$ in 1 M H_2SO_4 aqueous electrolyte. Additionally discussed in this report are the probabilities of $2p_{3/2} \rightarrow 5d$ electronic transitions pertaining to Eu^{III} and Eu^{II} ions. Implications for the use of XANES in studying intermediate-valence materials, and some potential applications of the presently reported spectroelectrochemical cell are described.

1. Introduction

XAFS (X-ray absorption fine structure) spectroscopy has found widespread application for *in situ* studies of systems of electrochemical interest. The combination of XAFS and electrochemical methods provides direct insights about electroactive species that are otherwise unavailable through use of the individual techniques alone. For example, XAFS spectroelectrochemistry has been used to probe the coordination and chemistry of adsorbed species, electrode/electrolyte interfaces, insoluble oxide films produced by passivation and corrosion, battery electrode materials, electrocatalysts, electrochemically-generated complexes in solution, etc.[1–7]. The investigation of these fundamental phenomena for emerging practical devices and new applications has been facilitated by the development of novel electrochemical cells that have proven to be suitable for a variety of XAFS measurements under electrochemically-relevant conditions [8–25].

Based upon the science of interest, it is important to utilize the appropriate spectroelectrochemical cell design to address the issues in question. The first solution cells employed for *in situ* XAFS spectroelectrochemistry had a thin-layer working electrode design that facilitated rapid, exhaustive electrolysis of small analyte volumes, about 500 μl [9, 10]. Thin-layer XAFS spectroelectrochemistry was also demonstrated with a 340 μl cell of similar design for low-energy X-ray studies of biological materials [21]. A flow-cell, bulk electrolysis system for *in situ* XAFS with a large analyte capacity (~ 10 ml) was recently shown to be effective for controlling the oxidation state of transition metal ions in complexes such as $[Co(2,2'\text{-bipyridine})_3]^{n+}$, for $n = 2$ and 3 [11].

For particular study topics such as the redox behaviour of lanthanide cations and heteropolyoxometalate anions in aqueous electrolytes, we have designed and built an electrochemical cell that is suitable for *in situ* XAFS data acquisition during bulk electrolysis at controlled potentials. In this report, this new, bulk electrolysis spectroelectrochemical cell design is described. The performance of the cell has been evaluated through europium L_3-edge XANES (X-ray absorption near edge structure) measurements during the course of the constant potential reduction of Eu^{III} to Eu^{II} in an aqueous solution. The europium (III,II) system has a simple and well-understood equilibrium behaviour as given in the potential–pH diagram [26]. Experimentally, the standard reduction potential ($E°$) for Eu^{III}/Eu^{II} (–0.55 V vs Ag/AgCl) is attainable in aqueous, non-complexing supporting electrolytes [27–30]. As such, the Eu(III,II) redox couple serves as a good model system to demonstrate the performance of this spectroelectrochemical cell design.

The design reported here is the result of our effort to produce a versatile, easy-to-use cell of intermediate analyte volume (~ 5 ml) with the following pivotal feature. This design utilizes two separate compartments for the working and auxiliary electrodes, and the auxiliary electrode compartment is kept away from the X-ray beam path so that this cell can be used

* Author to whom correspondence should be addressed.

0021-891X

in either fluorescence or transmission modes. As added conveniences, the following were considered in the design: (i) It is compatible for direct operation with commercially-available XAFS equipment, such as housings, detectors, slits and filters that are now in widespread use at many synchrotron radiation facilities throughout the world. (ii) It can operate under anaerobic or aerobic conditions with aqueous or nonaqueous supporting electrolytes for fluorescence XAFS above 2 keV and transmission XAFS above 35 keV. To realize these features, we departed from most of the previous state-of-the-art, thin-layer/parallel-plate cell designs to the parallel-rod cell design shown in Figure 1. The premise of this work, was to verify the *in situ* performance of the presently reported cell by using the Eu^{III}/Eu^{II} redox system. In the following, details of the key features of the *in situ* cell design and the europium L_3-edge XANES data obtained from the cell are presented.

2. Experimental details

2.1. *Electrochemical cell design*

A drawing of the solution spectroelectrochemical cell assembled for bulk electrolysis and *in situ* XAFS experiments is shown in Fig. 1. There are three main components of this design: (i) the solution cell (H) with its attachments (A–E, I–K, M); (ii) the cell positioner (N) with the cell attachments (A–D); and (iii) the cell box (F) with its components (G, L, O). A complete description of the items (A–O) illustrated in Fig. 1, including the principal dimensions, is provided in Table 1. The working (A) and auxiliary (D) electrodes are held in the cell body (H) and in the cell positioner (N) by four nylon male connectors (part no. NY-6MO-1-2BT, 6 mm tube to 1/8 inch pipe thread, Swagelok). The separation between the centres of the two graphite rods (A and D) is ~ 38 mm. The holes in the aluminium positioner (N) provide ample clearance to prevent contact with the electrodes.

The reference electrode (E) port in the cell (H) was drilled for a slip fit. The electrode (Model MF-2063, BAS) was held at the proper depth with an O-ring seal (not shown). The reference (E) electrode was placed in close proximity (less than 5 mm) to the working electrode (A). Note that, for this study, a chloride-containing reference electrode (E) was placed directly in the working electrode compartment. Although this direct immersion of a chloride-containing reference electrode in an electrochemical cell is a highly discouraged practice in most electrochemical studies, it is permissible for the present study because the electrolyte of interest contains chloride ions from the chloride salts of rare-earth or transition-metal cations. However, for other applications where contamination of the electrolyte or complication of the electrode process by Cl^- are of concern, the reference electrode can be placed outside the cell and connected to a Luggin capillary inside the cell (H) through a cracked stopcock bridge. Alternatively, a non-chloride based reference electrode (e.g., Ag/Ag_xS_y, $Cu/CuSO_4$, Hg/HgO, reversible hydrogen electrode etc.) can be used in place of the presently used Ag/AgCl reference electrode.

The two male connectors on the cell positioner (N) permit the vertical alignment of the X-ray beam on the cell window (J). The positioner (N) can be rotated

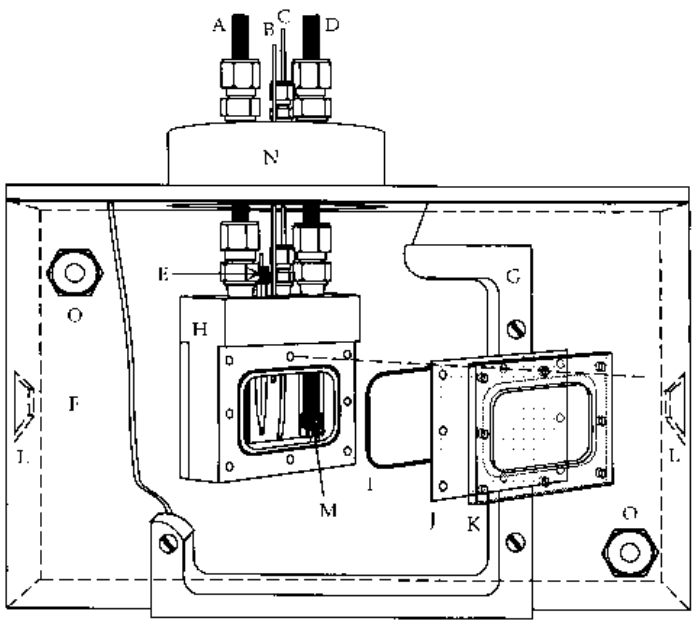

Fig. 1. Assembly drawing of the spectroelectrochemical system for *in situ* XAFS measurements. (A) Working electrode; (B) Electrolyte feed tube and gas vent port; (C) Purge gas feed tube; (D) Auxiliary electrode; (E) Reference electrode; (F) Cell box; (G) Bracket for mounting a fluorescence detector (not shown); (H) Spectroelectrochemical cell; (I) O-ring seal; (J) Cell window; (K) Window frame; (L) X-ray windows; (M) Auxiliary electrode compartment; (N) Cell positioner; (O) Cell box purge ports. In this view, the spectroelectrochemical cell is shown at a 45° angle, as it would be used for fluorescence XAFS measurements with the incident X-ray beam entering the cell box from the right. For clarity, the eight screws (4–40 × 1 in., Allen head and nuts) for mounting the cell window and the back side window disassembly are not shown.

Table 1. Descriptions, part numbers (where available), quantities (Qty), and principal dimensions of items A–O used for the fabrication of the XAFS spectroelectrochemical cell shown in Fig. 1

Items	*Part no.*	*Description*	*Qty*
A, D	14739	Carbon rod, 6.15 mm d. × 300 mm, purity grade "F"; material grade AGKSP (Alfa)	2
B, C	Z11731-5	Syringe needle, 20-gauge Teflon™, 12 in. long, with Kel-F Luer Hub (Aldrich)	2
E	MF-2063	Ag/AgCl reference electrode (5.5 cm × 6 mm o.d.) with porous Vycor™ tip and 3 M NaCl, RE-5 (BAS)	1
F		Cell box (8–9/16 × 5-1/4 × 3–7/16 in.), aluminium, with removable Plexiglas cover	1
G		Detector bracket (4–7/16 × 4–7/16 × 1 in.), aluminium, to support fluorescent ion chamber detector	1
H		Cell body (2–3/8 × 2–3/8 × 1/2 in.), Kel-F	1
I	AS-568A	O-ring, Kalrez, K#031, compound 4079, 1–3/4 × 1–7/8 × 1/16 in. (DuPont)	2
J	3522	Polycarbonate Window Film, 0.20 mil thick (SPEX)	2
K		Cell window frame (2–3/8 × 1–25/32 × 5/32 in.), Plexiglas	2
L		Slot (2–1/2 × 5/16 in.), covered with polycarbonate window film (item J)	2
M	7205-SP-10MMD	Fritted cylindrical sealing tube, porosity D, 10 mm o.d. (Ace Glass)	1
N		Cell positioner (2–13/16 i.d. × 3–1/16 in. o.d.), aluminium	1
O	268-P-04 × 02	Male connector, Poly-Flow (Imperial Eastman), 1/4 in. tube to 1/8 in. pipe thread	2

through 360° to allow adjustment of the angle between the cell and the incident X-ray beam. Once aligned, the positioner (N) can be locked down with two chocks (not shown) located on the top of the box (F). The connecting lead wire (not shown) for reference electrode connection was brought down to the reference electrode pin (1.5 mm dia.) through a feed port (not shown) in the cell positioner (N). The Teflon™ feed tube (C) for gas purging is held in the cell positioner (N) and the cell (H) by two nylon male connectors (part no. NY-100-1-1BT, 1/16 inch tube to 1/16 inch pipe thread, Swagelok). The drilled-through holes in the cell positioner (N) and the cell (H) were of adequate clearance to facilitate easy insertion of the Teflon™ feed tube (C). With the tube (C) withdrawn above solution level, the electrolyte can be blanketed with any gas or gas mixture. Alternatively, with the tube (C) inserted into the solution, the electrolyte can be purged. The gas vent/electrolyte feed tube (B) was brought through the cell positioner (N) with a slip fit hole and through the cell (H) with a press fit hole. The tube (B) is used for filling the cell and for venting the purge gas and other gases that may be produced at the electrodes during the electrolysis.

As the key feature of the presently reported cell, the compartment (M) for the auxiliary electrode (D) was made of glass to stand off the bottom of the cell (H) by ~2 mm. Five equally-spaced arches were formed at the end of the tubular auxiliary electrode compartment (M). These open slots provide low resistance current passage. The glass frit (pore dia. 10–20 μm) in the bottom end of the auxiliary electrode compartment (M) prevents the direct mixing of the electrolytes between the working (A) and auxiliary electrode (D) compartments. The auxiliary compartment tube (M) fits snugly within the 1 inch vertical opening in the cell (H). O-ring seals (I) were pressed into the channels on both sides of H (only one side is shown in Fig. 1) to provide a leak-tight seal of the window film (J) with the cell (H). The use of Kalrez O-ring seals, although costly, provided the most reliable leak-tight seals. Other materials, especially rubber, were more prone to swelling and cracking by the use of aggressive supporting electrolytes. The window frame (K) had a raised (~ 0.8 mm) rim on the inside surface that mated with the cell (H) to provide a snug, snap fit of the window film (J) into the cell (H). The window film was secured by the window frame (K) with eight screws (4–40 × 1 inch, Allen head) and nuts (not shown). We found that 5 μm thick polycarbonate film provides satisfactory chemical resistance for the duration of this study and, at the same time, has excellent transmission characteristics (≥ 95%) for all X-radiation above 2 keV [31]. Previously, we have used this film as a sample window for phosphorus *K*-edge (2130 eV) as well as cesium *K*-edge (35 985 eV) XAFS and have obtained satisfactory results [32, 33]. For more aggressive electrolytes and prolonged experimentation, other commercially available films such as Kapton™, Mylar™, etc. are suggested as the window material. The position and height of the X-ray entrance/exit windows (L) in the cell box (F) were machined to match the position and height of the windows in a commercially available housing (The EXAFS Co.), which was designed to contain a reactor/furnace for *in situ* XAFS studies of heterogeneous catalysts under industrially-relevant conditions [34].

The mounting bracket (G) was designed to provide an exact fit with a commercially available fluorescent X-ray ion chamber detector (The EXAFS Co., not

shown). This bracket can be substituted with a soller slit assembly (The EXAFS Co.). Directly behind the mounting bracket (G), on the inside of the box, are two vertical guides (not shown) that are used to accommodate large area fluorescence filters (10 cm × 10 cm) that are commercially available (e.g., EXAFS Materials). The cell box (F) has two purge ports (O) so that it can be flooded with appropriate gases or gas mixtures.

2.2. *Apparatus and reagents*

A potentiostat (model CV-27, BAS) was used for the constant-potential electrolysis of a 14.2 mM $EuCl_3 \cdot 6H_2O$ (99.99%, Aldrich) solution in a 1 M H_2SO_4 (Optima grade, Fisher Scientific) aqueous supporting electrolyte prepared with distilled-deionized water (18 MΩ cm). This solution (7 ml) was injected into the spectroelectrochemical cell where it was purged with helium prior to and throughout the course (~ 7 h) of electrolysis and *in situ* XANES measurements. The He purge tube was brought down into the electrolyte near the base of the working electrode at the back of the cell. Contrary to our initial concern, [23, 24, 35] this bubbler configuration provided satisfactory, noise-free X-ray absorption measurements. This is because the position of the bubbler tube was well behind (~ 1 cm) the X-ray irradiated volume. Moreover, since the 1/e escape depth of the Eu $L\alpha$ fluorescence radiation (5 817–5 846 eV) in the electrolyte is merely 0.4 mm, the bubbles rising some 1 cm away did not interfere with the *in situ* X-ray measurements. To our advantage, the He bubbles served to stir the electrolyte so that the species of interest is distributed uniformly in the entire volume of the electrolyte.

From the open circuit potential (+0.4 V vs Ag/AgCl), the electrode polarization was stepped to −0.7 V vs Ag/AgCl for the bulk electrolysis experiment. This potential, which is 0.15 V more negative than the standard reduction potential ($E°$) for the Eu^{III}/Eu^{II} couple [27], was chosen to achieve near-exhaustive electrolysis [36]. With this overpotential (−0.15 V), an equilibrium approximation from the Nernst equation suggests that the ratio of the concentrations, $[Eu^{II}]/[Eu^{III}]$, will be Ca. 340/1. For all practical purposes, this ratio can be considered as the representation of a near–exhaustive (>99.5%) electrolysis. All quoted potentials in this report are given with respect to a silver/silver chloride (SSC) reference electrode in a 3 M NaCl aqueous solution. During the electrolysis process, the illumination of the spectroelectrochemical cell with the X-ray beam was observed to have no measurable effect on either the control or measurement of the current and potential.

2.3. *XANES data collection*

Europium L_3-edge (6 977 eV) XANES was collected at ambient temperature on beamline X-23A2 at the National Synchrotron Light Source (NSLS) operating with 110-220 mA of electron current. X-23A2 is equipped with a Si<311> double crystal monochromator, which provides an energy resolution of $\delta E/E = 2.90 \times 10^{-5}$ [37], and effective harmonic rejection of the second order Bragg reflection. The feedback system was adjusted to provide ~ 90% of the maximum incident X-ray intensity I_0 (to suppress third order harmonic contamination) throughout the Eu L_3-edge scan. Nitrogen was used to monitor I_0. Helium was used to purge the cell box (i.e., the spectroelectrochemical cell was bathed in a He atmosphere) to reduce the absorption and scattering of I_0 and the fluorescent (I_f) X-radiation. The europium fluorescence signal was detected by use of a flow-type ion chamber detector (The EXAFS Co.), which was purged with argon and used without slits or a scattered radiation filter. This is a common approach with the conventional 45 °-incident/45 °-exit fluorescence XAFS configuration, which minimizes the scattered radiation entering the detector. Furthermore, for low-energy fluorescence XAFS, use of slits and filters is often impractical because of too large an attenuation of the fluorescence signals [38, 39].

With post-monochromator slits in the X-23A2 hutch, the vertical beam height and the horizontal beam width on the cell window were adjusted to be 1 mm × 15 mm, respectively. The cell position was adjusted so that the X-ray beam illuminated the electrolyte in the working electrode compartment through the polycarbonate window. Based upon the 1/e escape depth (0.4 mm) of the Eu $L\alpha$ fluorescence radiation, the total volume examined with the incident X-ray beam was 1 mm × 15 mm × 0.4 mm. With a 1 mm premonochromator vertical entrance slit, a total energy bandwidth of 1.1 eV at 7000 eV was calculated from the square root of the quadratic sum of the monochromator rocking curve width ($2\delta E^2 = 0.082$ eV) and the X-ray beam divergence ($\Delta E^2 = 1.2$ eV) [39]. Because the instrumental resolution (1.1 eV) is some 3.5 times smaller than the natural linewidth (3.91 eV) of the Eu L_3 core hole [40], the Eu L_3-edge XANES reported here is only slightly broadened (~ 4%) by the instrumental factors.

The *in situ* XANES was recorded, first, at the open circuit potential and, then, throughout the course of the electrolysis with the electrode polarized at –0.7 V vs SSC. The L_3-edge region was scanned with a step size of 0.3 eV/pt at 4 s/pt. A single scan from 6850 to 7620 eV took 32 min. The scan-to-scan energy calibration was maintained to ±0.2 eV. The calibration was set with reference to the inflection point energy (6980.3 eV) determined from the first derivative, transmission XANES of a standard EuF_3 absorber (EXAFS Materials). The calibration was run at regular intervals throughout the course of experimentation. The normalization of the XANES to a unit edge jump was performed according to conventional methods [39]. The pre-edge (6850–6955 eV) background was approximated by a two-term linear function, and the post-edge (7000 –7600 eV) back-

ground was approximated by a three-term quadratic function. As described elsewhere [34, 41–45], the normalized XANES was fit with the sum of Lorentzian and arctangent functions convolved with a 1.2 eV Gaussian broadening function to account for the effect of the X-ray beam divergence.

3. Results

The spectra of Fig. 2 display the evolution of the Eu L_3-edge XANES during the course of 7 h electrolysis of the aqueous solution of $EuCl_3.6H_2O$ in the spectroelectrochemical cell shown in Fig. 1. The normalized Eu XANES (Spectrum 1, Fig. 2) for this colourless, deaerated solution at open circuit potential reveals a single, intense edge resonance at 6981.6 eV. It is characteristic of Eu^{III}, which has the descriptive ground state electronic configuration of $[Xe]4f^65d^06s^0$. The resonance is the result of an electronic transition from the Eu $2p_{3/2}$ manifold to the empty 5d manifold. With the commencement of electrolysis at –0.7 V vs SSC, a series of XANES measurements was begun. In Fig. 2, XANES data (spectra 2 and 3) at two intermediate times are included with the sole intention of demonstrating the evolution of the Eu^{II} response with the progression of electrolysis. With the presently used conventional XAFS data acquisition technique, a time-resolved study is impractical especially at the beginning of the electrolysis, considering the 32 min of time required to collect a data set. For better time resolution, other techniques such as energy-dispersive XAFS measurements may be considered.

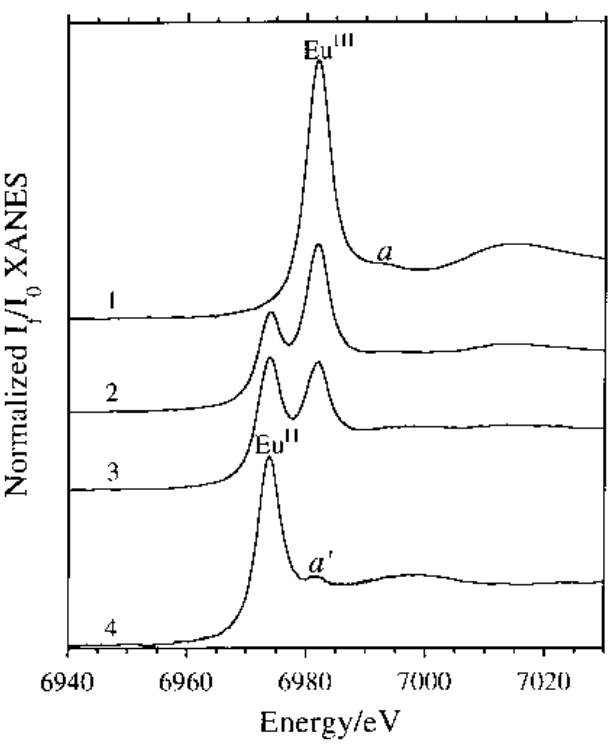

Fig. 2. *In situ*, europium L_3-edge XANES spectroelectrochemistry of $EuCl_3.6H_2O$ (14.2 mM) in an aqueous supporting electrolyte of 1 M H_2SO_4. At open circuit potential (+0.4 V vs SSC), spectrum 1. After bulk electrolysis with the electrode polarized at –0.7 V vs SSC for 1.2 h (spectrum 2), 2.8 h (spectrum 3), and 7.0 h (spectrum 4). The Eu^{III} and Eu^{II} edge peaks occur at 6981.6 and 6973.6 eV, respectively. The weak features labelled *a* and *a′* are assigned to photoelectron scattering resonances (i.e., EXAFS).

After electrolysis for 1.2 h, a new and well-resolved edge resonance is seen at 6973.6 eV (spectrum 2, Fig. 2). With longer electrolysis times (e.g., 2.8 h; spectrum 3), this resonance intensity increases at the expense of the intensity of the Eu^{III} resonance at ~ 6982 eV. The new edge resonance, which is 8 eV below the Eu^{III} resonance, is characteristic of Eu^{II} [46–51], which has the $[Xe]4f^75d^06s^0$ electronic configuration. After 7 h of electrolysis, the Eu^{II} resonance (spectrum 4, Fig. 2) dominates the spectrum. Although there is what appears to be some indication of residual Eu^{III} from the weak feature labelled *a′* at ~ 6982 eV in Fig. 2, we could not entirely rule out the possibility that *a′* arises from a photoelectron scattering event (i.e., EXAFS) caused by the structure of the Eu–O coordination polyhedron. Support for this assignment, which suggests that *a′* is not indicative of Eu^{III}, is provided by the Eu L_3-edge XANES studies of Tan *et al.* [52, 53]. They show that the presence of a feature similar to *a′* observed in this study is determined by the near-neighbour oxygen environment of europium.

From the data of Fig. 2, it is clear that Eu L_3-edge XANES provides direct information about the valence of Eu in solution. The fits to the normalized XANES for the pure Eu^{III} solution and the Eu^{II} solution after near-exhaustive electrolysis are displayed in Fig. 3 along with the individual components of the fits. The results of the curve fitting for the Eu^{II} and Eu^{III} oxidation states as well as for one of the $Eu^{II,III}$ mixtures ($t = 2.8$ h; spectrum 3, Fig. 2) are listed in Table 2. As mentioned before, the data for the intermediate times are included for the sole purpose of demonstrating the evolution of Eu^{II} with the progression of electrolysis.

4. Discussion

As demonstrated by the *in situ* Eu L_3-edge XANES of Fig. 2, which reveals the evolution of the reduction of Eu^{III} during electrolysis for ~ 7 *h*, the reported cell design permits experiments to reach exhaustion. In order to achieve this, it was essential to separate the working and auxiliary electrodes [36]. This was accomplished by use of an auxiliary electrode compartment separated from the working electrode compartment by a glass frit. This provides isolation of anolyte and catholyte and, thereby, prevents the direct intermixing of the anode reaction products (e.g., Eu^{III} from reoxidation of Eu^{II}, Cl_2, O_2) with the cathode reaction products (e.g., Eu^{II}, H_2). The resulting X-ray fluorescence signal is only then a true representation of the analyte under investigation.

For the $Eu^{III} + e^- \rightarrow Eu^{II}$ reaction as followed here, the cathodic reduction product (e.g., Eu^{II}) was illuminated within the working electrode compart-

Table 2. Europium L_3-edge peak intensities of the normalized XANES displayed in Fig. 1 and the results (positions, heights, FWHMs, areas, offsets) from the curve-fitting analyses of the normalized XANES[*]

	Eu^{III}/Eu^{II} Edge resonances				*Edge steps*				
Time[†]	*Intensity*	*Position*	*Height*	*FWHM*	*Area*	*Position*	*Height*	*FWHM*	*Offset*
BE[‡]	4.15 /	6981.9 /	4.33 /	4.70 /	32.0 /	6986.4	0.78	7.30	–0.09
2.8	2.05 / 2.12	6981.8 / 6973.7	1.81 / 2.03	5.88 / 4.28	16.7 / 13.7	6987.0	1.10	6.74	–0.07
7.0[§]	/ 3.04	/ 6973.7	/ 3.08	/ 4.33	/ 21.0	6977.0	1.03	5.30	–0.06

[*]The Eu^{III} and Eu^{II} edge resonances, due to $2p_{3/2}\rightarrow 5d$ bound-state electronic transitions, were modelled with Lorentzian functions and the absorption edge steps were modelled with arctangent functions by use of the algorithm of Lytle *et al.* (EDGFIT) [34, 41]. A second Lorentzian function was added to approximate the post-edge (EXAFS) peaks in order to provide better fits to the overall spectra obtained before electrolysis (BE) and after 7 h of electrolysis, see Fig. 3.

[†] Times are in hours from the start of the electrolysis with the electrode polarized at –0.7 V vs SSC.

[‡] Solution of Eu^{III} before electrolysis (BE) at open circuit potential.

[§] Solution of Eu^{II} at the end of electrolysis.

ment. The diffusion of Eu^{II} to the auxiliary electrode, where re-oxidation to Eu^{III} would occur, and also the diffusion of Eu^{III} back into the working electrode compartment were restricted by the frit separator. Because of the glass wall of the auxiliary electrode compartment, any anode reaction products (*e.g.*, Eu^{III}, O_2, Cl_2,) within the auxiliary electrode compartment did not interfere with the XAFS measurements. Also, the separator (glass frit) restricts the diffusion of anolyte into the working electrode compartment. If the two electrodes were not separated, intermixing of anode and cathode reaction products would alter the electrolyte composition and prevent the electrolysis from approaching completion. By comparison, with a thin-layer, parallel plate electrode cell geometry, X-radiation could illuminate both the working and auxiliary electrode plates and would sample both the cathode and anode reaction products. This would be problematic because the resulting spectral response would be a sum of both the anolyte and catholyte signals; the exact extent of the combination of different responses depends upon the energies of the incident/transmitted and fluorescent X-radiation as well as the position of the auxiliary electrode. Also, for redox systems whose equilibrium potentials vary with pH, use of small electrolyte volumes without any buffering capability can produce ambiguous results due to rapid pH swings, especially near the region of hydrogen evolution.

Although the 14.2 mM analyte (Eu) concentration examined here seems rather high for analytical electrochemistry, the data of Fig. 2 demonstrate that it is a practical concentration for the acquisition of good quality XANES in a single scan. In view of the stability of Eu^{II} as well as the attainable standard reduction potential for Eu^{III} ($E^\circ = -0.55$ V vs SSC in acid solution [27, 30]), this solution system provided a reliable test of the new spectroelectrochemical cell. We have used this cell for other *in situ* XANES studies as well. For example, *in situ* XANES was obtained for several lanthanide (*Ln*)-exchanged heteropolyoxotungstate anions of composition $[LnP_5W_{30}O_{110}]^{n-}$ [42, 54]. For the Eu^{III}-exchanged anion (5 mM in an aqueous electrolyte of 1 M H_2SO_4), we demonstrated that europium is electroactive and reducible to Eu^{II} by electrolysis at –0.55 V vs SSC [54]. Although the cell finds widespread application for fluorescence measurements, the back cell window is X-ray transparent to permit transmission XAFS measurements. The disadvantage here is that the fixed cell body thickness, ~ 1.2 cm, restricts its use for transmission XAFS to high energy experiments, such as for the *K*-edge of Cs (35 985 eV) and beyond. In fact, from proof-of-concept measurements conducted at SSRL with a Si<4 0 0> monochromator on beamline 4-2, we have demonstrated that this cell provides the ideal absorber thickness for Cs *K*-edge transmission XAFS of 0.1 M aqueous solutions of $CsNO_3$ and CsCl [32].

The Eu XANES data reported here were all obtained from the same dilute analyte in aqueous solution. Because of the low absorber concentration, the peak intensities are not vitiated by thickness effects, which can oftentimes cause serious distortions of intense $L_{2,3}$-edge resonances when obtained from concentrated, solid-state samples [39, 55]. Therefore, the curve fitting of the Eu L_3-edge XANES of Fig. 2 yields quantitative information about the resonance energies, widths, and intensities – all of which provide insights about the electronic properties of the absorbing Eu ion. The 8 eV difference in the europium edge-resonance energies between the solution species at open circuit potential before electrolysis and at −0.7 V vs SSC after electrolysis is sufficient to assign the oxidation states of Eu^{III} at the open circuit condition and Eu^{II} in the reduced solution. This interpretation of the XANES results is consistent with a variety of other published studies of Eu compounds [46–51, 56]. The difference in Eu^{III}–Eu^{II} edge-resonance energies is also in line with that observed for the Ln^{III} and Ln^{II} L_3 XANES of other lanthanide (*Ln*) ions, including Nd, Sm, and Yb [57–60]. Similarly, a 7–9 eV difference has been previously observed between Eu^{II} and Eu^{III} resonances in Eu $3d_{5/2}$ XPS (X-ray photoelectron spectroscopy) data [61–63].

The integrated intensity of an L_3-edge resonance is proportional to its oscillator strength, which includes a radial dipole-moment integral as well as the density of 5d states with the appropriate symmetry [41, 64]. It has been previously reported that the width of an

L_3-edge resonance varies inversely with the ionic volume of the lanthanide [56, 65], presumably through changes in the radial component of the oscillator strength. Rescaling the relative Eu^{III} and Eu^{II} energies, by a squared-ratio of their ionic radii (1120 and 1300 pm, respectively, for CN = IX [66]), to account for this volume effect, produces a trivalent linewidth similar to that observed for the divalent ion. Therefore, the increased linewidth of the Eu^{III} resonance over that of the Eu^{II} resonance observed in this study (given in Table 2) is attributed primarily to the difference in the ionic volume of these two ions. As seen from Figure 3, and shown in Table 2, the intensity of the electronic transition for Eu^{III} is also considerably larger than that for Eu^{II}.

Whereas the decreased radial integral for Eu^{II} against Eu^{III} is expected to decrease the observed intensity, differences in the density of 5d final states will also play a role. Eu^{III} has a $4f^6 5d^0$ configuration. It has been clearly demonstrated that there is very little 4f–5d hybridization or configuration mixing in this ion [67]. The 4f valence states are separated by about 8.5–9 eV from the unoccupied 5d states. However, for the Eu^{II} ion ($4f^7 5d^0$), the outer electrons are subjected to a much smaller effective nuclear charge, which results in much smaller separations between configurations. The 4f–5d separation in Eu^{II} has been found to be about 2.5 eV for the free ion [67, 68]. The effect of the crystal field is also larger for the divalent europium f-ion, and is expected to be of the same order as the free-ion splitting. These combined effects result in significant 4f–5d hybridization for Eu^{II}, giving some f character to the 5d states. This reduces the density of empty final-states with the symmetry appropriate for the L_3-edge transition, thereby contributing to the decrease in observed intensity of the Eu^{II} resonance compared to that of the Eu^{III} resonance.

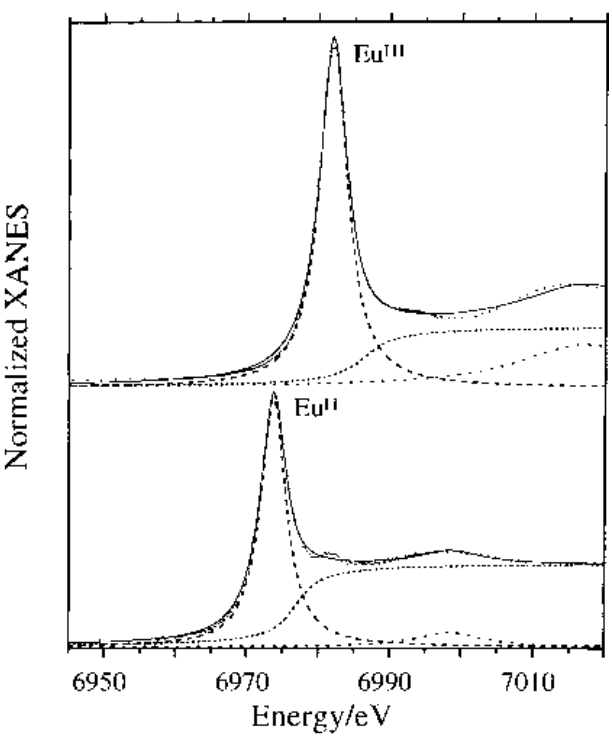

Fig. 3. The normalized XANES (dots) for the 14.2 mM aqueous solution of $EuCl_3.6H_2O$ in 1 M H_2SO_4 obtained at open circuit potential (Eu^{III}, top) and after constant potential bulk electrolysis for 7 h with the electrode polarized at –0.7 V *vs* SSC (Eu^{II}, bottom). The fits to the data are shown as solid lines and the individual Lorentzian and arctangent components of the fits are shown as dashed lines.

Whereas the larger ionic radius and the increased hybridization of the Eu^{II} ion are *both* expected to contribute to the decrease in the observed intensity of the Eu^{II} L_3-edge-resonance over that of the Eu^{III} resonance, their relative effects cannot be ascertained without further work. The observation of a decreased amplitude for the Eu^{II} resonance has been previously reported by Ravot *et al.* [48], who note that the amplitude of the Eu L_3-edge-resonance in Eu^{II}-oxide, EuO, is about 1.5 times smaller than that for Eu^{III}-oxide, Eu_2O_3. This ratio is similar to the one reported here in Table 2. Further support for a difference between Eu^{II}/Eu^{III} L_3-edge-resonance intensities is indicated from a study in which relative Eu^{II}/Eu^{III} concentrations were estimated from both L_3-edge XANES and ^{151}Eu Mössbauer spectra. The relative Eu^{II}/Eu^{III} concentrations obtained from the XANES data were found to be different from those obtained from the Mössbauer data [69].

Our results reported here provide unambiguous evidence of the decreased L_3-edge absorption intensities observed for Eu^{II} over that of Eu^{III} because the XANES data were obtained *on the same sample*. This is a particularly important result because XANES studies are used to determine the fractional valence in Eu homogeneous mixed-valent systems. These studies often rely on the assumption that the transition probabilities of the Eu^{II} and Eu^{III} are the same (see, for example, Rohler [56]). The work reported here shows that this assumption is not valid.

Finally, we would like to comment on the potential applications of the presently reported *in situ* cell for purposes other than that reported here. In many cases, the electrochemical process occurring at the very surface of the electrode is of great interest. However, in some systems such as the corrosion of iron or steel, it is also important to understand the dissolved species in order to comprehensively describe the mechanism of corrosion [70, 71]. In this regard, by using metal electrodes and an electrolyte that is electrochemically relevant to the environment of interest, this cell can be used to investigate the dissolution process and dissolved species during the corrosion process. Also, similar experiments can be designed to investigate the processes of electrocleaning, electroplating or conversion coating. [72, 73].

5. Conclusions

This europium L_3-edge XANES work has clearly demonstrated the *in situ* spectroelectrochemical per-

formance of the cell, specifically designed for characterization of solution species. Undoubtedly, the separation of working and auxiliary electrodes led the electrolysis to the point of near-exhaustion, and furthermore the separation made the XANES data free of compositional interferences due to reaction products from the auxiliary electrode reactions. The L_3-edge XANES measurements presented unambiguous evidence of the decreased L_3-edge absorption intensities observed for Eu^{II} over that of Eu^{III} because the XANES data were obtained *on the same sample*. This is a particularly important result because XANES studies are used to determine the fractional valence in Eu homogeneous mixed-valent systems. These studies often rely on the assumption that the transition probabilities of Eu^{II} and Eu^{III} are the same. The present work shows that this assumption is not valid.

Acknowledgements

We thank D. Sutter, G. Ktistou and J. Gregar (ANL) for their expert fabrication of this spectroelectrochemical cell. A part of this research was conducted at the National Synchrotron Light Source, which is supported by the US Department of Energy, Division of Material Sciences and Division of Chemical Sciences. This work was supported by the US D.O.E., Basic Energy Sciences – Chemical Sciences, under contract W-31-109-ENG-38.

References

[1] H. D. Abruna, G. M. Bommarito and H. S. Yee, *Acc. Chem. Res.* **28** (1995) 273.
[2] H. D. Abruna (Ed.), 'Electrochemical Interfaces. Modern Techniques for *In Situ* Interface Characterization', VCH, New York (1991).
[3] H. D. Dewald, *Electroanalysis* **3** (1991) 145.
[4] M. Froment (Ed.), 'Passivity of Metals and Semiconductors', Elsevier, Amsterdam (1983).
[5] L. R. Sharpe, W. R. Heineman and R. C. Elder, *Chem. Rev.* **90** (1990) 705.
[6] Proceedings of the Symposium on X-ray Methods in Corrosion and Interfacial Electrochemistry, vol. **92-1** (edited by A. J. Davenport and J. G. Gordon, II), The Electrochemical Society, Pennington, NJ (1992).
[7] 'Structure of Surfaces and Interfaces as Studied Using Synchrotron Radiation', Faraday Discussions of The Chemical Society, vol. **89**, The Royal Society Of Chemistry, London (1990).
[8] H. D. Dewald, J. W. Watkins, II, R. C. Elder and W. R. Heineman, *Anal. Chem.* **58** (1986) 2968.
[9] D. A. Smith, M. J. Heeg, W. R. Heineman and R. C. Elder, *J. Am. Chem. Soc.* **106** (1984) 3053.
[10] D. A. Smith, R. C. Elder and W. R. Heineman, *Anal. Chem.* **57** (1985) 2361.
[11] D. H. Igo, R. C. Elder, W. R. Heineman and H. D. Dewald, *Anal. Chem.* **63** (1991) 2535.
[12] D. H. Igo, R. C. Elder and W. R. Heineman, *J. Electroanal. Chem.* **314** (1991) 45.
[13] R. C. Elder, C. E. Lunte, A. F. M. M. Rahman, J. R. Kirchhoff, H. D. Dewald and W. R. Heineman, *ibid.* **240** (1988) 361.
[14] F. Villain, V. Briois, I. Castro, C. Helary and M. Verdaguer, *Anal. Chem.* **65** (1993) 2545.
[15] H. Yoshitake, O. Yamazaki and K. Ota, *J. Electroanal. Chem.* **371** (1994) 287.
[16] Z. Nagy, H. You, R. M. Yonco, C. A. Melendres, W. Yun and V. A. Maroni, *Electrochim. Acta* **36** (1991) 209.
[17] M. E. Herron, S. E. Doyle, K. J. Roberts, J. Robinson and F. C. Walsh, *Rev. Sci. Instrum.* **63** (1992) 950.
[18] M. E. Kordesch and R. W. Hoffman, *Nucl. Instrum. Meth. Phys. Res.* **222** (1984) 347.
[19] T. W. Capehart, D. A. Corrigan, R. S. Conell, K. I. Pandya and R. W. Hoffman, *Appl. Phys. Lett.* **58** (1991) 865.
[20] J. McBreen, W. E. O'Grady, K. I. Pandya, R. W. Hoffman and D. E. Sayers, *Langmuir* **3** (1987) 428.
[21] F. A. Schultz, B. J. Feldman, S. F. Gheller, W. E. Newton, B. Hedman, P. Frank and K. O. Hodgson, *in* 'Redox Mechanisms and Interfacial Properties of Molecules of Biological Importance', vol. **93-11** (edited by F. A. Schultz and I. Taniguchi), The Electrochemical Society, Pennington, NJ (1993) pp. 108–17.
[22] S. Kim, I. T. Bae, M. Sandifer, P. N. Ross, R. Carr, J. Woicik, M. R. Antonio and D. A. Scherson, *J. Am. Chem. Soc.* **113** (1991) 9063.
[23] D. A. Tryk, I. T. Bae, Y. Hu, S. Kim, M. R. Antonio and D. A. Scherson, *J. Electrochem. Soc.* **142** (1995) 824.
[24] D. A. Tryk, I. T. Bae, D. Scherson, M. R. Antonio, G. W. Jordan and E. L. Huston, *ibid.* **142** (1995) L76.
[25] D. A. Tryk, S. Kim, Y. Hu, W. Xing, D. A. Scherson, M. R. Antonio, V. Z. Leger and G. E. Blomgren, *J. Phys. Chem.* **99** (1995) 3732.
[26] M. Pourbaix, 'Atlas of Electrochemical Equilibria in Aqueous Solutions', 2nd edn, Cebelcor, Brussels (1974) pp. 183–97.
[27] L. B. Anderson, D. J. Macero, *J. Phys. Chem.* **67** (1963) 1942.
[28] G. Biedermann and G. S. Terjosin, *Acta Chem. Scand.* **23** (1969) 1896.
[29] G. Biedermann and H. B. Silber, *ibid.* **27** (1973) 3761.
[30] A. J. Bard, R. Parsons and J. Jordon, 'Standard Potentials in Aqueous Solution', Marcel Dekker, New York (1985) p. 834.
[31] 'SPEX Handbook of Sample Preparation and Handling', 4th edn (edited by R. H. Obenauf, R. Bostwick, M. McCann, J. D. McCormack, R. Merriman and S. Selem), SPEX Sample Preparation: Metuchen, NJ (1994) Ch. 4.
[32] M. R. Antonio, M. Dietz, M. Jensen, L. Soderholm and E. P. Horwitz, *Inorg. Chim. Acta* (1996) in press.
[33] M. R. Antonio, *in* 'XAFS Workshop: SRI'94', Stony Brook, NY (1994).
[34] F. W. Lytle, R. B. Greegor and E. C. Marques, *in* Proc. 9th Int. Congr. Catal. Calgary, vol. 5 (edited by M. J. Phillips and M. Ternan), The Chemical Institute of Canada: Ottawa (1988) pp. 54–85.
[35] S. Kim, D. A. Tryk, M. R. Antonio, R. Carr and D. Scherson, *J. Phys. Chem.* **98** (1994) 10269.
[36] A. J. Bard and L. R. Faulkner, 'Electrochemical Methods. Fundamentals and Applications', John Wiley & Sons, New York (1980) Ch. 10.
[37] T. Matsushita and H. Hashizume, *in* Handbook on Synchrotron Radiation', vol. 1A (edited by E. E. Koch), North-Holland, Amsterdam (1983) pp. 261–314.
[38] F. W. Lytle, R. B. Greegor, D. R. Sandstrom, E. C. Marques, J. Wong, C. L. Spiro, G. P. Huffman and F. E. Huggins, *Nucl. Instrum. Methods Phys. Res.* **226** (1984) 542.
[39] F. W. Lytle, *in* 'Applications of Synchrotron Radiation', vol. 4 (edited by H. Winick, D. Xian, M. H. Ye and T. Huang), Gordon & Breach, New York (1989) pp. 135–223.
[40] M. O. Krause and J. H. Oliver, *J. Phys. Chem. Ref. Data* **8** (1979) 329.
[41] F. W. Lytle, *Ber. Bunsenges. Phys. Chem.* **91** (1987) 1251.
[42] M. R. Antonio and L. Soderholm, *Inorg. Chem.* **33** (1994) 5988.
[43] M. R. Antonio, J. S. Xue and L. Soderholm, *J. Alloys Compounds* **207/208**, (1994) 444.
[44] U. Staub, M. R. Antonio, L. Soderholm, M. Guillaume, W. Henggeler and A. Furrer, *Phys. Rev. B: Condensed Matter* **50** (1994) 7085.
[45] J. S. Xue, M. R. Antonio, W. T. White, L. Soderholm and S. M. Kauzlarich, *J. Alloys Compounds* **207/208** (1994) 161.
[46] F. J. Berry, J. F. Marco and A. T. Steel, *Hyperfine Interactions* **83** (1994) 347.
[47] G. V. Bazuev, L. D. Finkel'shtein, N. D. Samsonov and G. P. Shveikin, *Russian J. Inorg. Chem.* **32** (1987) 158.

[48] D. Ravot, C. Godart, J. C. Achard and P. Lagarde, *in* 'Valence Fluctuations in Solids' (edited by L. M. Falicov, W. Hanke and M. B. Maple), North-Holland, Amsterdam (1981) pp. 423–26.
[49] G. Michels, S. Junk, W. Schlabitz, E. Holland-Moritz, M. M. Abd-Elmeguid, J. Dünner and A. Mewis, *J. Phys.: Condensed Matter* **6** (1994) 1769.
[50] G. Wortmann, *Hyperfine Interactions* **47** (1989) 179.
[51] G. Wortmann, I. Nowik, B. Perscheid, G. Kaindl and I. Felner, *Phys. Rev. B: Condensed Matter* **43** (1991) 5261.
[52] Z. Tan, J. I. Budnick, W. Q. Chen, D. L. Brewe, S. W. Cheong, A. S. Cooper and L. W. Rupp, Jr., *ibid.* **42** (1990) 4808.
[53] Z. Tan, J. I. Budnick, S. Luo, W. Q. Chen, S. W. Cheong, A. S. Cooper, P. C. Canfield and Z. Fisk, *ibid.* **44** (1991) 7008.
[54] M. R. Antonio and L. Soderholm, *J. Cluster Sci.* (1996) in press.
[55] G. Meitzner, G. H. Via, F. W. Lytle and J. H. Sinfelt, *J. Phys. Chem.* **96** (1992) 4960.
[56] J. Röhler, *in* 'Handbook on the Physics and Chemistry of Rare Earths', vol. 10 (edited by K. A. Gschneidner, Jr., L. Eyring and S. Hüfner), North-Holland, Amsterdam (1987) pp. 453–545.
[57] J. P. Lelieur, J. Goulon, R. Cortes and P. Friant, *J. Phys. Chem.* **88** (1984) 3720.
[58] R. K. Singhal and K. B. Garg, *J. Magn. Magn. Mater.* **116** (1992) 238.
[59] F. Lissner, K. Krämer, T. Schleid, G. Meyer, Z. Hu and G. Z. Kaindl, *Anorg. Allg. Chem.* **620** (1994) 444.
[60] T. Baba, S. Hikita, R. Koide, Y. Ono, T. Hanada, T. Tanaka and S. Yoshida, *J. Chem. Soc., Faraday Trans.* **89** (1993) 3177.
[61] E. J. Cho, S. J. Oh, S. Imada, S. Suga, T. Suzuki and T. Kasuya, *Phys. Rev. B: Condensed Matter* **51** (1995) 10146.
[62] M. Han, S. J. Oh, J. H. Park and H. L. Park, *J. Appl. Phys.* **73** (1993) 4546.
[63] W. D. Schneider, C. Laubschat, I. Nowik and G. Kaindl, *Phys. Rev. B* **24** (1981) 5422.
[64] L. F. Mattheiss and R. E. Dietz, *ibid.* **22** (1980) 1663.
[65] U. Fano and J. W. Cooper, *Rev. Modern Phys.* **40** (1968) 441.
[66] R. D. Shannon, *Acta Cryst.* **A32** (1976) 751.
[67] G. H. Dieke, 'Spectra and Energy Levels of Rare Earth Ions in Crystals', Interscience Publishers, New York (1968) p. 401.
[68] S. Hufner, 'Optical Spectra of Transparent Rare Earth Compounds', Academic Press, New York (1978) p. 237.
[69] G. Wortmann, W. Krone, E. V. Sampathkumaran and G. Kaindl, *Hyperfine Interactions* **28** (1986) 581.
[70] I. Song, M. R. Antonio and J. H. Payer, *J. Electrochem. Soc.* **142** (1995) 2219.
[71] I. Song, D. Gervasio and J. H. Payer, *J. Appl. Electrochem.* (1996) in press.
[72] S. L. Amey, G. M. Michal and J. H. Payer, *Metall. Mat. Trans A* **25A** (1994) 723.
[73] I. Song, J. H. Payer, R. Painter and M. Marzano, *Plat. Surf. Fin.* **82** (1995) 66.